Journal of Biomechanics xxx (2018) xxx–xxx

Contents lists available at ScienceDirect

Journal of Biomechanics

journal homepage: www.elsevier.com/locate/jbiomech
www.JBiomech.com

Investigation of the dependence of joint contact forces on musculotendon parameters using a codified workflow for image-based modelling

Luca Modenese [a,b,*], Erica Montefiori [a], Anqi Wang [c], Stefan Wesarg [c], Marco Viceconti [a], Claudia Mazzà [a]

[a] Department of Mechanical Engineering and INSIGNEO Institute for in silico Medicine, University of Sheffield, Sheffield, UK
[b] Department of Civil and Environmental Engineering, Imperial College London, UK
[c] Visual Healthcare Technologies, Fraunhofer IGD, Darmstadt, Germany

ARTICLE INFO

Article history:
Accepted 21 March 2018
Available online xxxx

Keywords:
Biomechanics
Musculoskeletal modelling
MR imaging
Musculotendon parameters
Joint contact forces
Juvenile gait

ABSTRACT

The generation of subject-specific musculoskeletal models of the lower limb has become a feasible task thanks to improvements in medical imaging technology and musculoskeletal modelling software. Nevertheless, clinical use of these models in paediatric applications is still limited for what concerns the estimation of muscle and joint contact forces. Aiming to improve the current state of the art, a methodology to generate highly personalized subject-specific musculoskeletal models of the lower limb based on magnetic resonance imaging (MRI) scans was codified as a step-by-step procedure and applied to data from eight juvenile individuals. The generated musculoskeletal models were used to simulate 107 gait trials using stereophotogrammetric and force platform data as input. To ensure completeness of the modelling procedure, muscles' architecture needs to be estimated. Four methods to estimate muscles' maximum isometric force and two methods to estimate musculotendon parameters (optimal fiber length and tendon slack length) were assessed and compared, in order to quantify their influence on the models' output. Reported results represent the first comprehensive subject-specific model-based characterization of juvenile gait biomechanics, including profiles of joint kinematics and kinetics, muscle forces and joint contact forces. Our findings suggest that, when musculotendon parameters were linearly scaled from a reference model and the muscle force-length-velocity relationship was accounted for in the simulations, realistic knee contact forces could be estimated and these forces were not sensitive the method used to compute muscle maximum isometric force.

1. Introduction

Musculoskeletal models are mathematical representations of the skeleton and musculature that through computer simulations allow the estimation of internal forces, such as muscle and joint articular forces, occurring within the human body during locomotion and not measurable without surgically-invasive procedures.

Various so-called "generic" lower limb musculoskeletal models, developed mainly using cadaveric data, have been proposed (Carbone et al., 2015; Delp et al., 1990; Modenese et al., 2011). Easier access to medical images and the emergence of dedicated software has now made it possible to generate subject-specific models with a high level of anatomical personalization (Taddei et al., 2012). Valente et al. (2014), for instance, assessed the robustness of a methodology for creating image-based subject-specific models using a software called NMSBuilder, which was proposed as standard tool for implementing OpenSim model generation workflows (Valente et al., 2017). Scheys et al. (2009) validated software to map musculotendon geometries from atlases of children with cerebral palsy into new models. However, due to the complexity of the topic and the absence of a commonly accepted and established workflow, a comprehensive description of the methodologies used to generate image-based patient specific models is still lacking, potentially compromising reproducibility (Erdemir et al., 2016) and hindering adoption in clinical practice.

Since comprehensive datasets of patients with implanted instrumented prostheses were made available (Fregly et al., 2012), several image-based subject-specific models of adult patients have been created and used with established biomechanical computational tools (Damsgaard et al., 2006; Delp et al., 2007)

* Corresponding author at: Room C+13 – INSIGNEO Institute for in silico Medicine, The University of Sheffield, The Pam Liversidge Building, Mappin Street, Sheffield, United Kingdom.
E-mail address: l.modenese@sheffield.ac.uk (L. Modenese).

https://doi.org/10.1016/j.jbiomech.2018.03.039
0021-9290/

to estimate knee articular forces (Gerus et al., 2013; Marra et al., 2015). However, very limited studies have focused on the estimation of internal forces in children using a subject-specific approach. Previous pediatric subject-specific models have been mainly used for estimating musculotendon lengths and moment arms (Hainisch et al., 2012; Scheys et al., 2008), joint kinematics (Kainz et al., 2016; Scheys et al., 2011) and muscle function (Correa et al., 2011), whereas previous walking simulations employed models with limited personalization of musculotendon geometries (Correa and Pandy, 2011) or estimated only the ankle joint contact forces (Hannah et al., 2017; Prinold et al., 2016). Nonetheless, image-based models seem highly desirable for investigating children gait biomechanics, due to the sensitivity of muscle force estimation to the muscle moment arms (Ait-Haddou et al., 2004; Herzog, 1992). The muscle moment arms significantly differ when estimated by scaling generic models using gait analysis data as opposed to subject-specific image-based models, both in healthy children and in children with cerebral palsy (Correa et al., 2011).

A critical aspect when creating image-based musculoskeletal models, is the identification of musculotendon parameters (namely, optimal fiber length l_o^m and tendon slack length l_s^t). In fact, such parameters cannot be derived directly from magnetic resonance imaging (MRI), whereas in principle muscle strength can be estimated using segmented muscle volumes or regression equations (Handsfield et al., 2014). Since previous extensive sensitivity studies, performed using generic models (Carbone et al., 2016; Navacchia et al., 2015; Scovil and Ronsky, 2006) showed these parameters can strongly affect muscle force generation, their effects within a subject-specific modelling approach should be assessed, especially if a complete modelling workflow has to be codified.

This paper aims to: (a) codify the generation of juvenile subject-specific musculoskeletal dynamics models, starting from medical imaging and motion capture data; (b) assess different methods for the identification of musculotendon architectural parameters to identify the most suitable techniques to include in our workflow.

2. Methods

2.1. Participants

To investigate the effects of modelling the muscle dynamics without confounding factors coming from pathological conditions, we focused on healthy children. The complexity of the imaging and instrumental protocol, however, made it unethical to run it in a juvenile population without a clinical justification. Hence we used data from a group of children with a previous history of Juvenile Idiopathic Arthritis (JIA) (Ravelli and Martini, 2007), who were enrolled within a larger clinical study run as part of the FP7 research project MD-Paedigree in various European pediatric hospitals. The study design involved three visits six months apart (M00, M06, M12), when a child's health status was assessed using clinical regional MRI scans (Malattia et al., 2013), ultrasound joint examination (Lanni et al., 2016; Roth et al., 2016), clinical gait analysis (Davis et al., 1991), and disease-specific clinical activity scores, e.g. JADAS (Consolaro et al., 2009). A child was deemed healthy at the time of the assessment if they were pain-free, showed no clinical or ultrasound signs of JIA activity, and no radiological signs of bone erosion or cartilage structural damage. Following these criteria, data from eight children (11 visits, 8 MRI and 11 clinical gait analysis datasets; 4 males and 4 females, age and anthropometry at each visit reported in Table 1) collected within MD-Paedigree for other purposes, were re-used for this study, with the approval of hospitals' research ethics committees.

2.2. Imaging and gait analysis data

MRI was used to acquire images of the lower limbs of each subject at the M06 visit. A 3D T1-weighted fat-suppression sequence (e-THRIVE) scanning sequence with 1 mm in-plane resolution and a 1 mm slice thickness was used to scan the entire lower limb in 5 stacks. This sequence allowed a scanning duration of around 10 min and hence favored pediatric applicability. The imaging protocol included positioning some MRI-visible skin markers on well-defined bony landmarks to allow registration between MRI and stereophotogrammetric data (Fig. 1 A and B). Gait analysis data were collected using a modified Vicon Plug-in-gait markers set (Fig. 1 B), employing an 8-camera stereophotogrammetric system (Vicon Motion System Ltd, Oxford, UK; 200 Hz), and two force plates (AMTI OR6-6; 1000 Hz).

2.3. Musculoskeletal models

A statistical shape model approach developed after Steger et al. (2012) was used to segment the MRI images and produce geometrical models of the lower limb bones and external skin surface. Meshlab (Cignoni et al., 2008) (http://www.meshlab.net) and Netfabb Basic (https://www.autodesk.com) were then used to group the bones and soft tissues belonging to each body segment

Table 1
Anthropometrics of participants as measured at the control visits where they were considered in healthy conditions. If the visit did not correspond with the full lower limb MRI data collection, variations of anthropometry, as recorded in the gait lab, are reported. For subjects whose mass varied by more than 3%, the inertial properties of the segments were updated. For subjects whose height varied by more than 3%, the model produced from MRI was uniformly scaled. Patient controls, i.e. the planned visits, were M00 (baseline), M06 (six month follow up) and M12 (12 months follow up).

Subj	Gender	From MRI collection (M06)		Gait data collection [control]	From gait data collection				
		Height [m]	Mass [kg]		Age	Height (variation)	Mass (variation)	Scaled segment lengths	Scaled inertial properties
S1	F	1.23	23.5	M12	8	1.35 (+10%)	28.5 (+21%)	Yes	Yes
S2	M	1.5	37	M06	10.5	–	–	–	–
S3	F	1.28	23	M12	8	1.30 (+2%)	26 (+13%)	No	Yes
S4	M	1.17	35.7	M06	7.5	–	–	–	–
S5	M	1.55	45.6	M06	12.5	–	–	–	–
S6	M	1.36	32	M06	10.5	–	–	–	–
		1.36	32	M12	11	1.42 (+4%)	37 (+16%)	Yes	Yes
S7*	F	1.55	54.5	M00	14	1.55 (<1%)	54.5 (<1%)	No	No
		1.56	54.5	M06	14.5				
		1.56	54.5	M12	15	1.55 (<1%)	54.5 (<1%)	No	No
S8	F	1.54	63.5	M12	14	1.54 (<1%)	67 (+5%)	No	Yes

* S7 was enrolled because previously affected by JIA, but was healthy for the entire duration of the study.

Please cite this article in press as: Modenese, L., et al. Investigation of the dependence of joint contact forces on musculotendon parameters using a codified workflow for image-based modelling. J. Biomech. (2018), https://doi.org/10.1016/j.jbiomech.2018.03.039

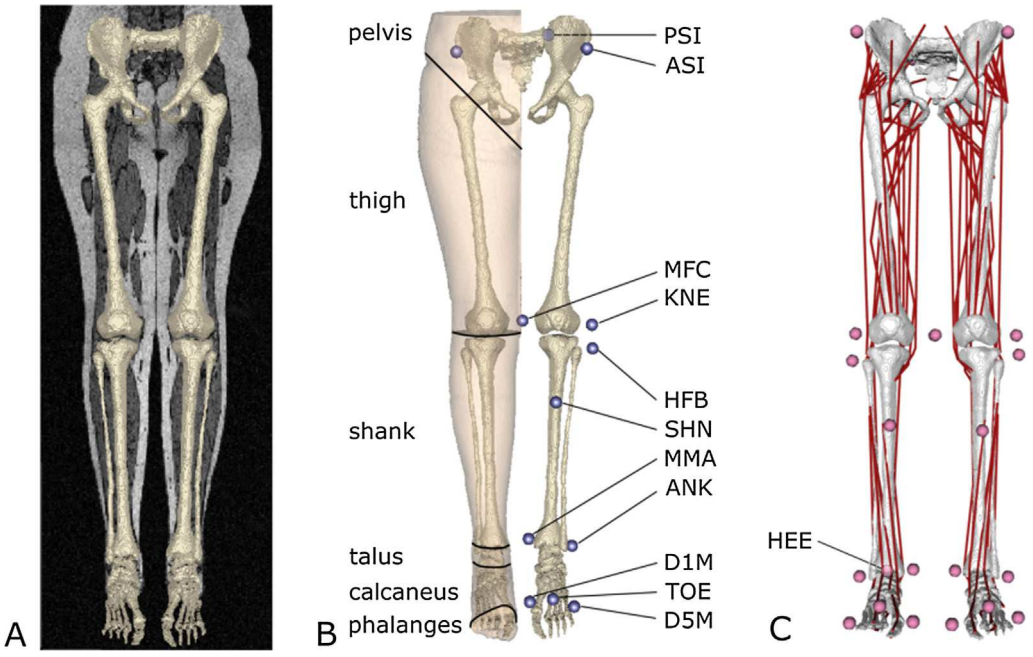

Fig. 1. (A) Bone geometries segmented from full lower limb MRI scans, (B) lower limb segments included in the lower limb model (left) and MRI-visible skin markers (right) (C) OpenSim model including musculotendon actuators and markers used for marker placement and for calculating joint angles. A marker placer procedure is used to place HEE in the OpenSim model by registering the markers available in the MRI with the static trial. MFC and D5M are not used for calculating the joint angles in dynamic trials. Please note that a metatarsophalangeal joint was included in the model, defined as a hinge with axis aligned with the line connecting the 1st and 5th distal metatarsal heads, but was not employed in the simulations for this study.

(Fig. 1 B). Inertial properties were calculated for each body segment using NMSBuilder (http://www.nmsbuilder.org), assigning different densities to bone (1.42 g/cm^3) and soft tissue (1.02 g/cm^3 for females, 1.03 g/cm^3 for males) (Dumas et al., 2005; White et al., 1987).

The lower limb skeletal model was created combining the functionalities of NMSBuilder and OpenSim. Joint parameters were identified by fitting analytical shapes to articular surfaces identified on the bone geometries in Meshlab. A sphere was fitted to the femoral head to model the hip joint as a ball and socket joint (3 Degrees Of Freedom, DOF), while cylinders were fitted to the posterior articular surface of the femoral condyles (Yin et al., 2015) and to the talar trochlea (Siegler et al., 2014) to identify the axes of hinge joint (1 DOF) for the tibiofemoral and talocrural joints, respectively. The models included a patella rigidly attached to the tibia, rotating around the knee axis. The axis of the subtalar joint (1 DOF hinge) was estimated joining the centers of two spheres fitted to the talocalcaneal and talonavicular articular surfaces (Parr et al., 2012). All fitting operations were least-squares procedures implemented in MATLAB (v8.5, R2015a, Mathworks, USA); the cylinder fitting relied on the LSGE MATLAB library (http://www.eurometros.org). Including a free joint between pelvis and ground (6 DOF), the bilateral model presented 18 DOF in total.

A detailed step-by-step description of the procedure is made available (see Appendix A).

2.4. Musculotendon geometry

The paths of 42 musculotendon actuators were defined through a supervised atlas registration procedure. For each segment of the generic model gait2392 (Delp et al., 1990), related muscle attachments (including via points) were grouped into an atlas. A set of well-defined (van Sint Jan, 2007), repeatable (Ascani et al., 2015) bony landmarks, constituting a landmark cloud, were then identified on the bone surface. Finally, these landmark clouds were registered onto the subject-specific bones using affine transformations (Horn, 1987) to match correspondent, virtually palpated (Taddei et al., 2007) bony landmarks. The subject-specific muscle attachments and via-points resulted from applying these transformations to the points in the muscle attachment atlases. Minor adjustments to the muscle paths, performed consulting sectional anatomy textbooks, e.g. Moller and Reif (2007), were usually necessary to finalize the muscle paths. The path points variability due to these adjustments was estimated in the order of 3.17 ± 2.16 mm in a pilot study where a single operator created, for three times, three MRI-based models from datasets not used in this study. The *peroneus tertius* was the only muscle from gait2392 not included in the model as not identifiable in the MRI. For six models built using the gait data collected when the MRI was not available, a uniform scaling procedure was applied using the anthropometric information available from the gait lab (Table 1).

All the above operations, performed in NMSBuilder (Valente et al., 2017), allowed the generation of an OpenSim model from each MRI dataset (Fig. 1 C).

2.5. Musculotendon architectural parameters

Musculotendon units were modelled using a dimensionless three element Hill-type muscle model (Thelen, 2003; Zajac, 1989), which requires the definition of five parameters: the optimal fiber length l_o^m, the tendon slack length l_s^t, the maximum isometric force F_{iso}, the maximum contraction velocity v_{max} and the fiber pennation angle at optimal fiber length α_o. Musculotendon parameters (l_o^m and l_s^t) were estimated using two distinct methods: M1, that maintains the l_o^m/l_s^t ratio of the generic gait2392 model (Delp et al., 1990), and M2, that aims to reproduce in the subject-specific model, for all combinations of joint angles in the sagittal plane, the same maximum isometric muscle contractile

Please cite this article in press as: Modenese, L., et al. Investigation of the dependence of joint contact forces on musculotendon parameters using a codified workflow for image-based modelling. J. Biomech. (2018), https://doi.org/10.1016/j.jbiomech.2018.03.039

conditions of the gait2392, i.e. the same normalized fiber and tendon lengths (Modenese et al., 2016; Winby et al., 2008).

For both M1 and M2, F_{iso} was computed using four different methods (F1-F4):

$$\text{F1} \quad F_{iso,SS} = \frac{M_{limb,SS}}{M_{limb,gen}} * F_{iso,gen} \tag{1}$$

$$\text{F2} \quad F_{iso,SS} = \frac{M_{SS}}{M_{gen}} \frac{l^{mt}_{gen}}{l^{mt}_{SS}} * F_{iso,gen} \quad \text{(Correa and Pandy, 2011)} \tag{2}$$

$$\text{F3} \quad F_{iso,SS} = \left(\frac{H_{SS}}{H_{gen}}\right)^2 * F_{iso,gen} \quad \text{(Steele et al., 2012b)} \tag{3}$$

$$\text{F4} \quad F_{iso,SS} = \frac{V_{SS}}{l^{m}_{o,SS}} * \sigma \quad \text{(Handsfieldet al.., 2014)} \tag{4}$$

In Eqs. (1)–(4), M is body mass, M_{limb} the lower limb mass, H body height, V the muscle volume, l^{mt} the musculotendon length, subscript *SS* indicates subject-specific, subscript *gen* indicates generic model and σ is the maximum muscle tension (set to 37 N/cm^2 in this study after Weijs and Hillen (1985)). In Eq. (4), V_{SS} is computed from the linear regressions of Handsfield et al. (2014) and used to estimate F_{iso} from the muscle physiological cross-sectional area (Lieber and Friden, 2000) neglecting the effect of muscle pennation angle, accounted for in the computational muscle model. The combinations of M1-M2 and F1-F4 led to eight different estimates of the muscle parameters. Finally, v_{max} was set to 10 fibers per second (Zajac, 1989) and α_o values were taken directly from the gait2392 model.

2.6. Biomechanical simulations

The biomechanical simulations were performed in OpenSim 3.3 (Delp et al., 2007) leveraging the MATLAB API and using single limb subject-specific models (11 DOF). Joint angles and moments were computed with the inverse kinematics and inverse dynamics OpenSim tools, respectively. The body and joint reference systems, based on ISB conventions (Wu et al., 2002), were defined using the bone geometries, whereas joint kinematics was computed tracking skin markers. This introduced an angular offset that depended on the joint axis definition, the subject pose during the MRI scans, and the location of the virtual markers in the model and the experimental skin markers. In spite of the impossibility of isolating the above different sources of variation, to facilitate – results' interpretation and make data from different models directly comparable, we decided to consider as zero the static posture joint angles. Joint powers were computed in MATLAB using angular velocities and inverse dynamics output. Muscle forces were estimated using a static optimization approach that, considering the physiological muscle force-length-velocity (F-L-V) relationship that regulates muscle force generation (Zajac, 1989), minimizes the sum of muscle activations squared. Ideal moment generators (reserve actuators), providing joint torque when muscle forces could not balance the external moments, were included for each DOF. Previous literature showed that the F-L-V relationship does not affect the static optimization results for a generic model (Anderson and Pandy, 2001). To verify whether this also applies to a subject-specific case, simulations were performed both with and without considering the F-L-V relationship. To prevent muscle recruitment alterations, reserve actuators were made unfavourable to recruit by assigning them a unitary maximum force, i.e. a provided joint torque of 1 Nm weighted on the static optimization objective function as much as a fully activated muscle. Finally, the "*JointReaction*" analysis in OpenSim (Steele et al., 2012a) was used to calculate the joint contact forces.

2.7. Quality assurance of simulations

The quality of the registration between the stereophotogrammetric landmarks trajectories to the subject-specific anatomical model derived from medical imaging was assessed by the peak tracking error over the entire markers' set, which, in agreement with best practices (Hicks et al., 2014), was ensured to be <20 mm for all the models.

The static optimization approach was verified by ensuring the contribution of reserve actuators to the joint dynamic equilibrium never exceeded 10% of the total joint moment over the entire gait cycle. This threshold was consistent with a previous study on a pediatric population (Steele et al., 2012b). The percentage of simulations discarded because of exceeding this threshold was then used as a metric to compare different modelling methods.

Additional quality checks to be performed on the experimental data, surface fitting and generated models are reported in the supplementary materials (step-by-step guide).

2.8. Statistical analysis of the results

Groups of simulation results were compared using Statistical Parameter Mapping (SPM). SPM relies on the Random Vector Field theory to account for data variability, allowing the comparison of group means for time-varying quantities. All analyses were done with MATLAB, using the *spm1d* package (Pataky et al., 2013).

The effect of the different methods used to estimate the maximum isometric force on the variability of the joint contact forces was evaluated with the SPM equivalent of a one-way ANOVA; the significance of individual differences between the joint reaction estimates was tested using the SPM equivalent of an unpaired Students' *t*-test. In all analyses the significance level was set to $\alpha = 0.05$.

3. Results

Two of the models had to be scaled to account for height changes and four to account for mass variations (details in Table 1) in the absence of MRI data at that particular control. In total, gait from 11 control visits were simulated (107 trials: speed: 1.08 ± 0.07 m/s, step length 1.18 ± 0.05 m, cadence: 55.1 ± 2.7 stride/min). Sagittal plane joint kinematics, moments and powers are presented in Fig. 2, out of sagittal plane results are available as supplementary materials.

Musculotendon parameters estimated using M1 resulted in consistently longer l^t_s and shorter l^m_o than those obtained by M2 (Fig. 3). The first three estimates of $F_{iso,SS}$ (F1-F2-F3) did not depend on musculotendon parameters, with F1 estimating the smaller $F_{iso,SS}$ and F3 the larger. F4 yielded the most variable $F_{iso,SS}$ because, despite estimated muscle volumes depended on M and H, large differences in l^m_o between M1 and M2 propagated to muscle strengths (Fig. 4).

As expected, no method achieved a 100% success rate in the verification of the muscle static optimization. Percentage of successful simulations are reported in Table 2 (see supplementary material for reserve moments). Hip internal/external rotation moment required intervention of reserve actuators most frequently, causing the majority of failures, followed by the ankle moment. M1 led up to 63–88% of successful simulations, while M2 (5–35% of successful simulations) resulted in models generally unable to provide the required ankle joint moment and was not further analyzed. The percentage of successful simulations decreased with decreasing

Please cite this article in press as: Modenese, L., et al. Investigation of the dependence of joint contact forces on musculotendon parameters using a codified workflow for image-based modelling. J. Biomech. (2018), https://doi.org/10.1016/j.jbiomech.2018.03.039

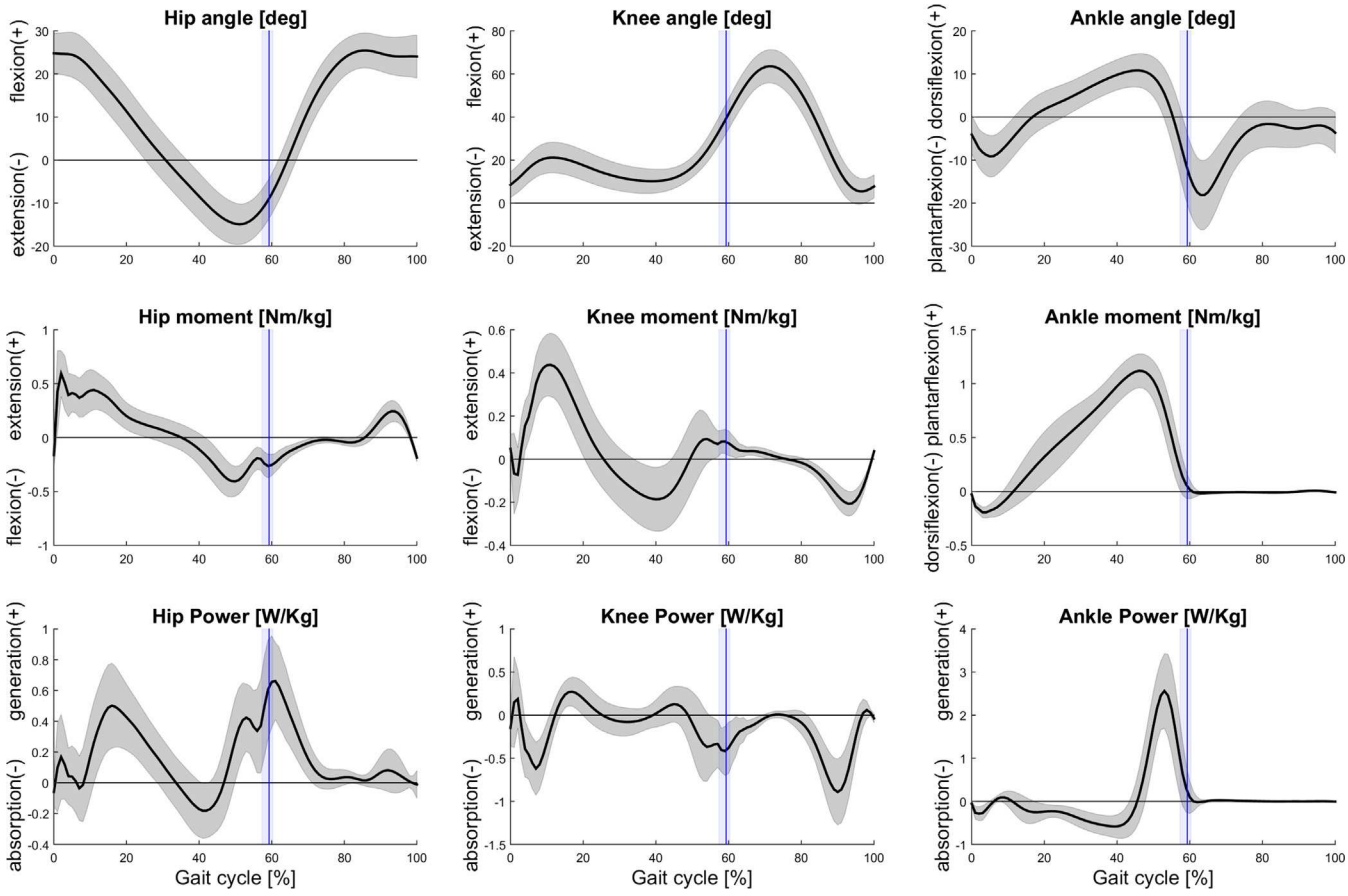

Fig. 2. Biomechanical variables (joint angles, joint moments and joint powers) estimated for the sagittal plane during walking of typically developing juvenile subjects. Joint angles are presented considering angles equal to zero for the static standing pose. Joint moments and joint powers are normalized by body mass. Curves are obtained from 107 walking strides of 8 subjects tested at 11 control visits. Complete results, including pelvis kinematics and non-sagittal degrees of freedom, are available as supplementary material.

estimation of $F_{iso,SS}$, while neglecting muscle F-L-V relationship entirely allowed more than 92% successful simulations. Results from M2 successful simulations are available in supplementary materials.

Joint reaction forces are presented for hip, knee and ankle joints in Fig. 5, combining all approaches to estimate musculotendon parameters and maximum isometric force, while peak values are summarized in Table 3. When the muscles' F-L-V relationship was not considered, the second peak of knee contact forces was larger than that computed accounting for F-L-V relationship ($p < 0.003$), reaching mean magnitudes of up to 3.2 times the subject's body weight (BW) for F1, F2 and F3 (see Table 3). Conversely, estimated joint contact forces at hip and ankle joints were found insensitive to the method used to estimate $F_{iso,SS}$ throughout the walking stance phase (no significant differences, $p > 0.05$, see web supplementary material).

4. Discussion

The first aim of this paper was to codify the generation of subject-specific musculoskeletal dynamics models, starting from medical imaging and motion capture data. We achieved this by proposing a methodology that combines various modelling approaches (Parr et al., 2012; Prinold et al., 2016; Valente, 2013; Valente et al., 2017; Yin et al., 2015) and enables a complete musculoskeletal analysis, making this the first study to present a comprehensive subject-specific model-based characterization of the gait biomechanics of a juvenile population, including profiles of internal forces computed from musculoskeletal models. To favor reproducibility and adoption of the proposed methodology, the atlas of muscle attachments and landmark clouds used in the registration, a detailed step-by-step description of the procedure, and the models used in this study are publically available (see Appendix A). It is worth noting that the described methodology relies entirely, with the exception of MATLAB, on freely available software. Whilst the examined cohort is too limited for the reported curves to be considered as normality curves, they can still be used by others as a reference to detect possible deviations from healthy patterns. In this respect, a shortcoming of the study is that participants were classified as healthy from a cohort of children previously affected by JIA. Although they were objectively assessed by clinical experts and none of them exhibited signs of persisting disease activity, minor motor compensation or recovering mechanisms could have still occurred.

In the proposed workflow, the knee and talocrural joints are modelled as hinges. More complex kinematic models (Parenti-Castelli and Sancisi, 2013) would have required identification of ligaments attachments, and therefore more detailed medical images to be personalized (Brito da Luz et al., 2017). The patellofemoral joint is also simplified compared to other approaches, e.g. Sancisi and Parenti-Castelli (2011). However, since no muscle path penetrated the bone geometries, the chosen simplification was considered satisfactory for the purposes of this study. Finally, the proposed multi-segmental ankle joint complex presents a stronger link to functional anatomy (Isman and Inman, 1968; Kapandji, 1987; Parr et al., 2012) than other subject-specific modelling

Please cite this article in press as: Modenese, L., et al. Investigation of the dependence of joint contact forces on musculotendon parameters using a codified workflow for image-based modelling. J. Biomech. (2018), https://doi.org/10.1016/j.jbiomech.2018.03.039

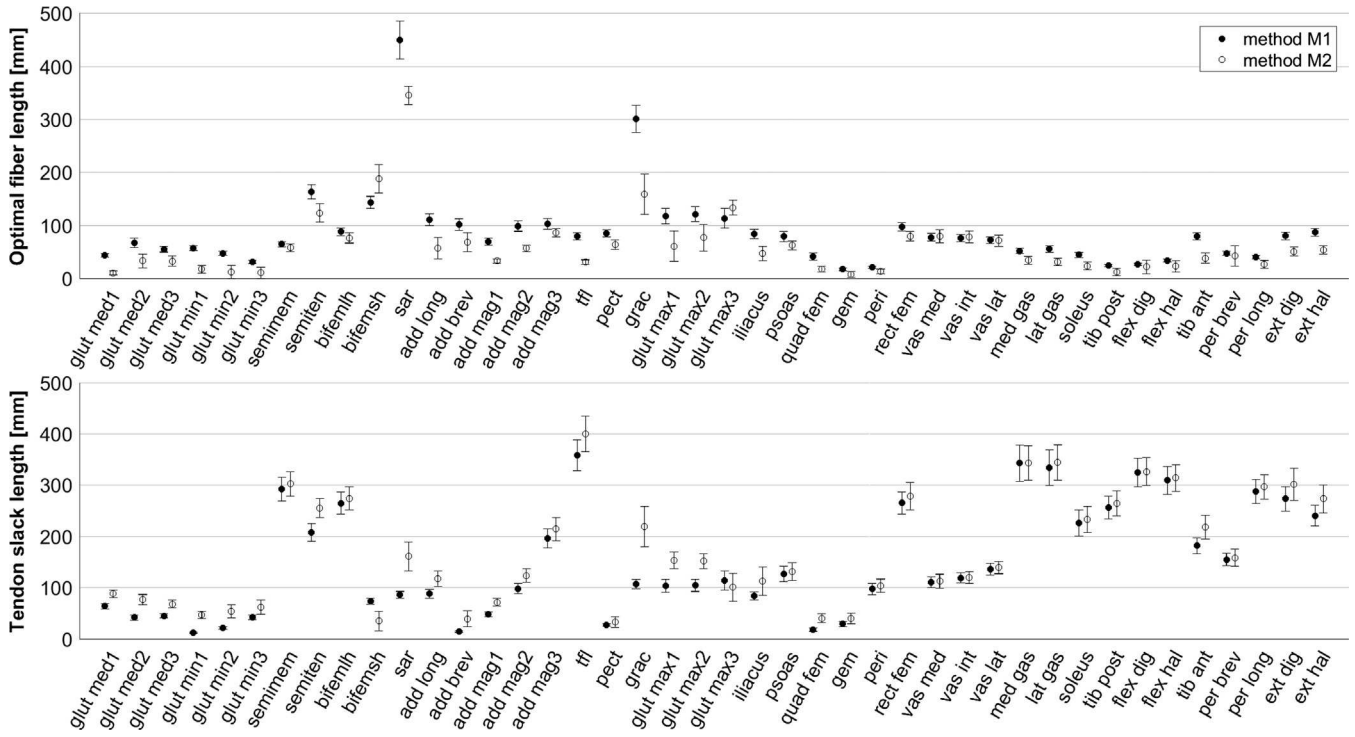

Fig. 3. Musculotendon parameters obtained maintaining the same ratio of optimal fiber length and tendon slack length of reference model gait2392 (method M1) and applying the method of Modenese et al. (2016) (method M2). Whiskers indicate plus/minus one standard deviation.

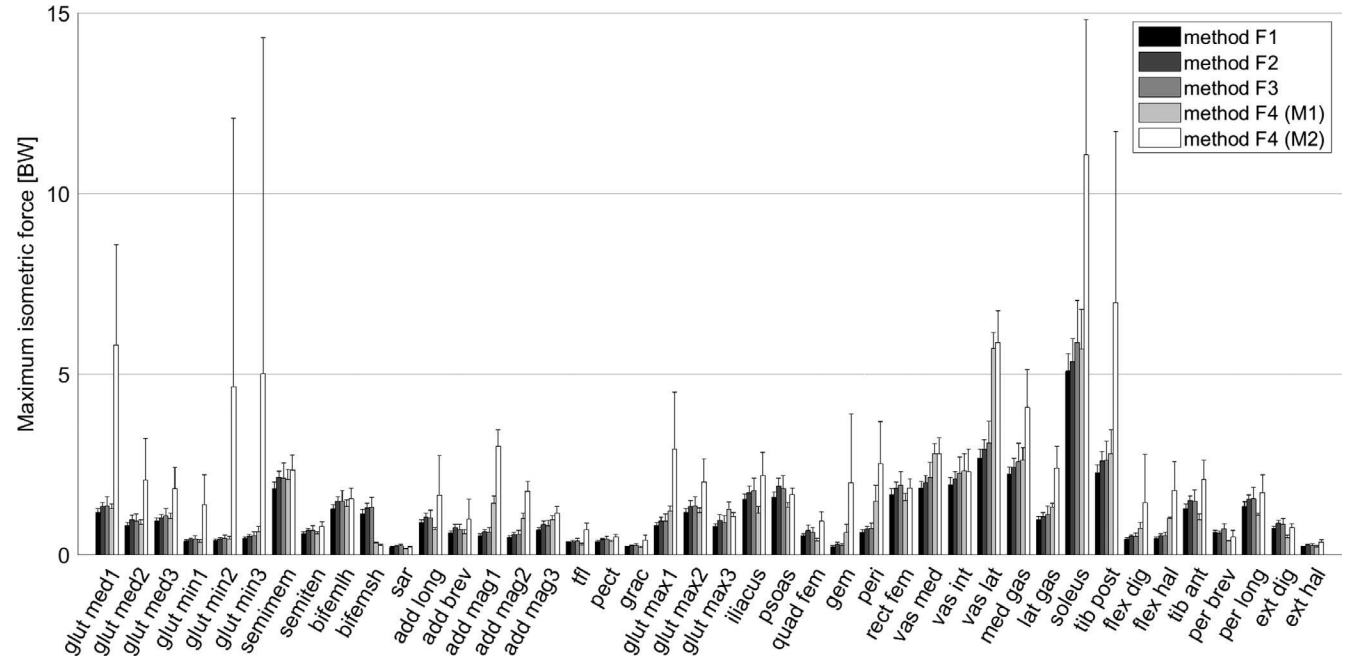

Fig. 4. Maximum isometric forces estimated for all muscles of the lower limb using four different methods (see Eqs. (1)–(4)). The estimations for method F4 depend on optimal fiber length, so they have been calculated for both M1 and M2.

approaches (Prinold et al., 2016; Saraswat et al., 2010) relying on models inspired to gait analysis (Stebbins et al., 2006), so enabling investigation of the subtalar joint kinematics (Montefiori et al., 2017).

The second aim of the paper was investigating the effect of different methods for the identification of the musculotendon architectural parameters on the models' predictions. Our findings confirmed that appropriate estimation of musculotendon parameters are essential for obtaining successful simulations. Method M2, which successfully predicted muscle parameters consistent with cadaveric measurements in a previous study (Modenese et al., 2016), was too sensitive to the differences between the generic and subject-specific models in terms of geometry of musculotendon paths, joint models and joint angle offsets, which are all elements compromising the resulting muscle function in the subject-specific model. This led to decreased muscle moment gen-

Please cite this article in press as: Modenese, L., et al. Investigation of the dependence of joint contact forces on musculotendon parameters using a codified workflow for image-based modelling. J. Biomech. (2018), https://doi.org/10.1016/j.jbiomech.2018.03.039

Table 2
Percentage of simulations for which reserve actuators contribute to the joint balance with <10% of the peak moment, reported for each degree of freedom of the model. When reserve actuators were below the 10% threshold at all joints, the simulation was considered successful. Note that maximum isometric forces for method F4 can be estimated only if musculotendon parameters have been computed, so only results considering the force-length-velocity relationship are presented.

		Method for maximum isometric force			
		Method F1	Method F2	Method F3	Method F4
Method M1	Hip flexion/extension	100	100	100	100
	Hip abduction/adduction	100	99	99	98
	Hip internal/external rotation	74	80	75	68
	Knee flexion/extension	100	100	99	100
	Ankle plantarflexion/dorsiflexion	88	95	98	96
	% successful simulations	**63**	**78**	**74**	**68**
Method M2	Hip flexion/extension	88	95	90	99
	Hip abduction/adduction	50	64	57	82
	Hip internal/external rotation	20	27	34	66
	Knee flexion/extension	76	80	76	94
	Ankle plantarflexion/dorsiflexion	8	14	13	51
	% successful simulations	**5**	**5**	**7**	**35**
No F-L-V relationship	Hip flexion/extension	100	100	100	–
	Hip abduction/adduction	100	100	100	–
	Hip internal/external rotation	92	93	92	–
	Knee flexion/extension	100	100	100	–
	Ankle plantarflexion/dorsiflexion	100	100	100	–
	% successful simulations	**92**	**93**	**92**	**–**

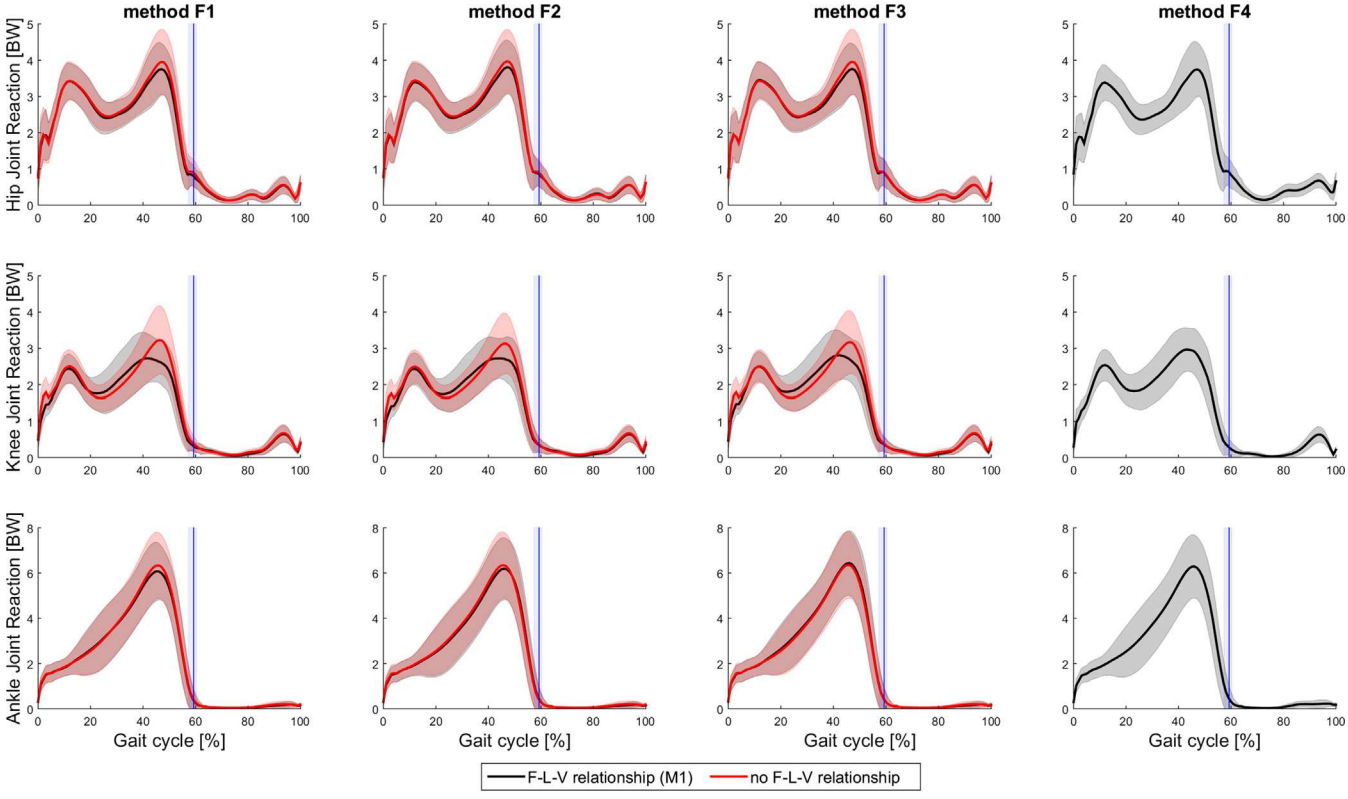

Fig. 5. Joint reaction forces at the hip, knee and ankle joints (rows) computed for the different methods used to estimate maximum isometric forces (columns) considering the force-length-velocity relationship with musculotendon parameters from method M1 (in black) and ignoring the force-length-velocity relationship (in red). Note that maximum isometric forces for method F4 can be estimated only if musculotendon parameters have been computed, so only results from simulations considering the force-length-velocity relationship are presented. (For interpretation of the references to colour in this figure legend, the reader is referred to the web version of this article.)

eration capacity and a small percentage of successful simulations. M1, however, yielded up to 88% of successful simulations.

Interestingly, the method chosen for estimating muscle strength did not affect the estimated joint contact forces, presenting magnitudes aligned with previous subject-specific simulations (Prinold et al., 2016; Valente et al., 2014). Nonetheless, this choice can strongly influence the percentage of successful simulations. Conversely, when neglecting the muscle F-L-V relationship almost all simulations were successful, but the computed second peak of knee contact forces was significantly larger than that estimated using M1. This peak reached mean values of 3.2 BW, i.e. around 0.5 BW larger than those measured in adults using instrumented prostheses (Fregly et al., 2012; Kutzner et al., 2010). This difference might be due to larger forces produced by the *rectus femoris* and

Table 3
Peaks of joint reaction forces at hip, knee and ankle joint (mean ± standard deviation) reported as function of the method used to estimate the musculotendon parameters and the maximum isometric force. Note that the number of successful simulations was not consistent between simulation techniques. Method M2 (Modenese et al., 2016) was not considered because of the small percentage of successful simulation.

		Method for estimation of maximum isometric force			
Joint reaction	Musculotendon parameters	Method F1	Method F2	Method F3	Method F4
Hip joint	Method M1	3.8 ± 0.7	3.8 ± 0.7	3.8 ± 0.7	3.7 ± 0.8
	No F-L-V relationship	4.0 ± 0.9	4.0 ± 0.9	4.0 ± 0.9	NA
Knee joint	Method M1	2.7 ± 0.7	2.7 ± 0.5	2.8 ± 0.7	3.0 ± 0.6
	No F-L-V relationship	3.2 ± 0.9	3.1 ± 0.8	3.2 ± 0.9	NA
Ankle joint	Method M1	6.1 ± 1.3	6.2 ± 1.4	6.4 ± 1.4	6.3 ± 1.4
	No F-L-V relationship	6.3 ± 1.5	6.3 ± 1.5	6.4 ± 1.5	NA

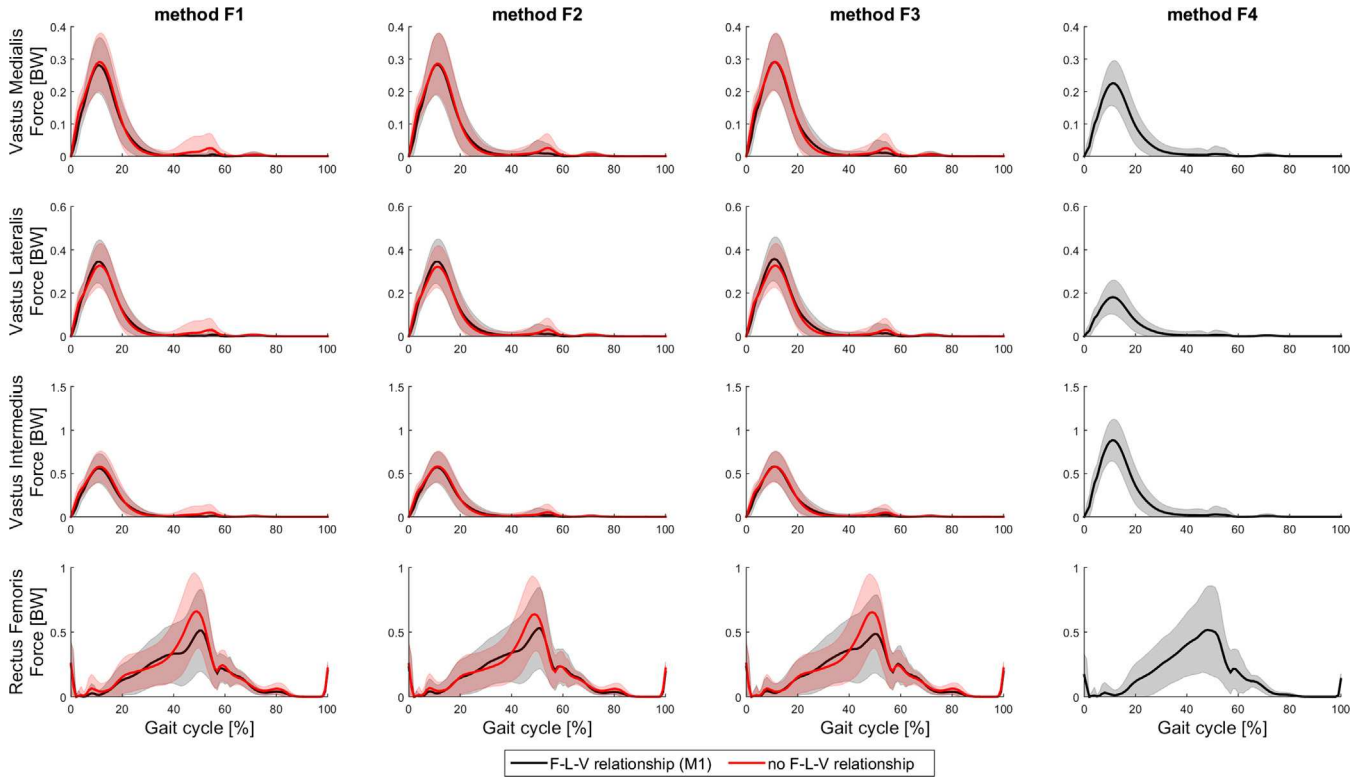

Fig. 6. Muscle forces of *vastus medialis*, *vastus lateralis*, *vastus intermedius* and *rectus femoris* (rows) computed for the different methods used to estimate maximum isometric forces (columns) considering the force-length-velocity relationship with musculotendon parameters from method M1 (in black) and ignoring the force-length-velocity relationship (in red). Note that maximum isometric forces for method F4 can be estimated only if musculotendon parameters have been computed, so only results from simulations considering the force-length-velocity relationship are presented. (For interpretation of the references to colour in this figure legend, the reader is referred to the web version of this article.)

gastrocnemii (Figs. 6 and 7) when the F-L-V relationship is neglected, i.e. neglecting the effect of the muscle contraction dynamics.

The proposed modelling methodology has some limitations. First, it relies on segmented bone geometries, and MRI segmentation is a time-consuming processing bottleneck. Nonetheless, promising developments in statistical shape modelling techniques (Zhang et al., 2014) and atlas based segmentations (Kolk et al., 2015) have been published recently. Excluding segmentation, an expert operator required around 10 h to generate a complete bilateral lower limb model, against 8–10 h reported by Prinold et al. (2016) for a foot and ankle model using similar procedures. Second, the supervised atlas registration is intrinsically limited by the fact that the atlas bony landmark clouds are identified on the simplified bone geometries of the gait2392 model. Whereas Valente et al., (2014) demonstrated the robustness of model output to variation in muscle attachments, Hannah et al. (2017) reported up to 24% of inter-operator variability for a foot and ankle model. Future work is needed to further automate musculotendon path generation and assess the repeatability of the procedure and the sensitivity of the model output to these variations. Additionally, future studies might focus on full validation and quantification of the accuracy of the model, possibly relying on data from instrumented prosthesis. Third, a direct comparison of predicted muscle activation against electromyographic signals could not be performed with the available data. As a consequence, M1 was preferred to M2 based on percentage of successful simulations, although both methods produced realistic results, with M2 yielding hip joint reactions closer to values measured *in vivo* (Bergmann et al., 2001) (see web supplementary results). An enhanced formulation of M2, robust against musculotendon path variations, could be preferable to M1 in the future. Finally, in the presented simula-

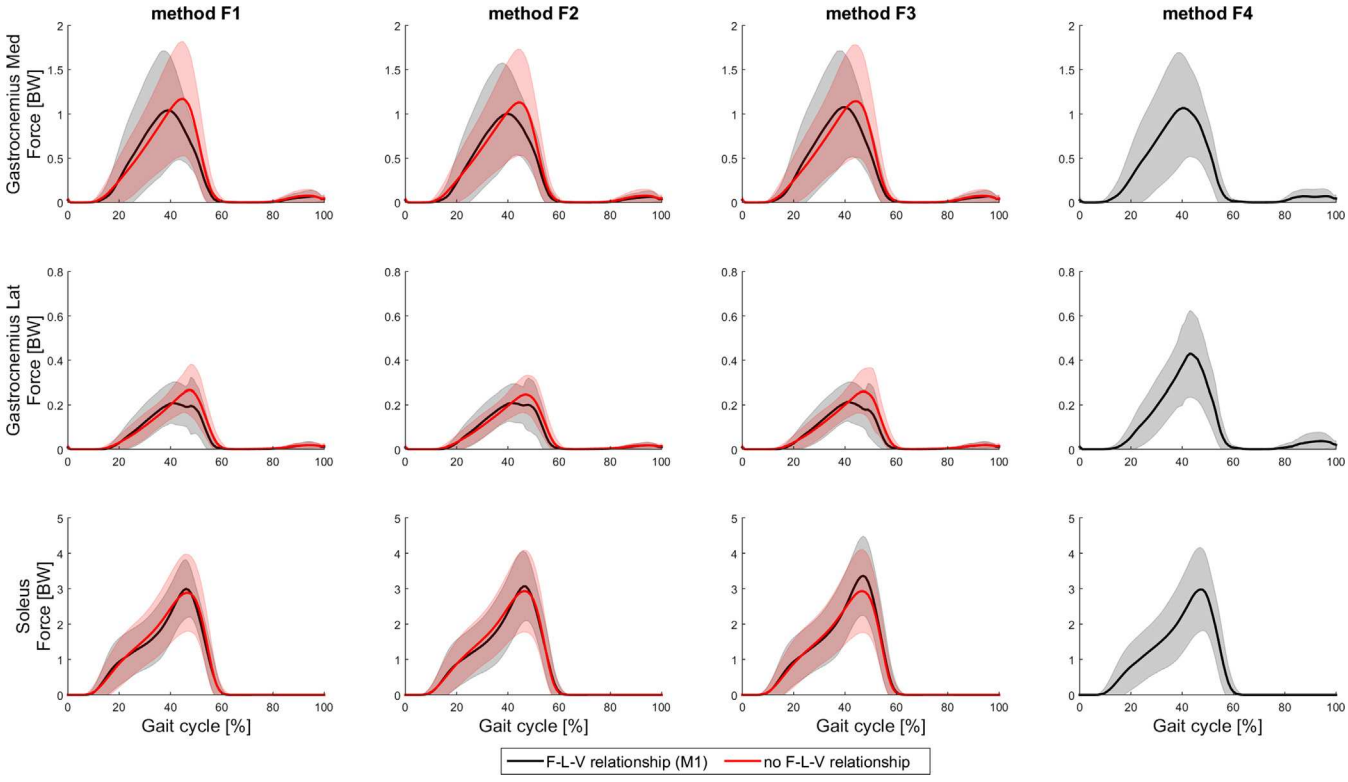

Fig. 7. Muscle forces of *gastrocnemius medialis, gastrocnemius lateralis* and *soleus* (rows) computed for the different methods used to estimate maximum isometric forces (columns) considering the force-length-velocity relationship with musculotendon parameters estimated from M1 (in black) and ignoring the force-length-velocity relationship (in red). Note that maximum isometric forces for method F4 can be estimated only if musculotendon parameters have been computed, so only results from simulations considering force-length-velocity relationship are presented. (For interpretation of the references to colour in this figure legend, the reader is referred to the web version of this article.)

tions, the muscle tendon was considered infinitely stiff and the passive muscle force was neglected. Consequently, reported findings might not extend to models including a compliant model of the tendon and considering passive muscle force.

In conclusion, this paper presented a methodology to create subject-specific models from medical images and applied it to a group of typically developing children. A complete analysis of their gait biomechanics, including muscle and articular forces that could serve as comparison for future studies on juvenile populations has been provided. By assessing different methods available in the literature, it was shown that musculotendon parameters can be estimated maintaining the ratio of tendon and fiber lengths from a generic model, maximum isometric force can be computed in different ways with little influence on final muscle force predictions and muscle force-length-velocity relationship should be considered in static optimization simulations to predict realistic knee contact forces. In the future, we plan to adapt the methods presented here to clinical populations, including children and adults with neurodegenerative diseases and musculoskeletal conditions such as osteoarthritis.

Conflict of interest

The authors declare that they do not have any financial or personal relationships with other people or organizations that could have inappropriately influenced this study.

Acknowledgments

This research was supported by the European Commission (MD-PAEDIGREE project, FP7-ICT Programme, Project ID: 600932), by the UK EPSRC (Multisim project, Grant number: EP/K03877X/1), and by the NIHR grant to support the NIHR Sheffield Biomedical Research Centre (Translational Neuroscience) (Grant number: IS-BRC-1215-20017). The authors would like to acknowledge Bart van Veen, Giuliano Lamberto, and Fabio Storm for the helpful discussion about several aspects of this study, and all the colleagues working at the pediatric hospitals participating in the MD-Paedigree project who contributed to the data collection.

Appendix A

The complete set of results, together with the documentation used to build the models is available as supplementary material at https://figshare.com/s/e371621054ff71049971.

Appendix B. Supplementary material

Supplementary data associated with this article can be found, in the online version, at https://doi.org/10.1016/j.jbiomech.2018.03.039.

References

Ait-Haddou, R., Jinha, A., Herzog, W., Binding, P., 2004. Analysis of the force-sharing problem using an optimization model. Math. Biosci. 191, 111–122.
Anderson, F., Pandy, M., 2001. Static and dynamic optimization solutions for gait are practically equivalent. J. Biomech. 34, 153–161.
Ascani, D., Mazzà, C., De Lollis, A., Bernardoni, M., Viceconti, M., 2015. A procedure to estimate the origins and the insertions of the knee ligaments from computed tomography images. J. Biomech. 48, 233–237.
Bergmann, G., Deuretzbacher, G., Heller, M., Graichen, F., Rohlmann, A., Strauss, J., Duda, G.N., 2001. Hip contact forces and gait patterns from routine activities. J. Biomech. 34, 859–871.

Brito da Luz, S., Modenese, L., Sancisi, N., Mills, P.M., Kennedy, B., Beck, B.R., Lloyd, D. G., 2017. Feasibility of using MRIs to create subject-specific parallel-mechanism joint models. J. Biomech. 53, 45–55.

Carbone, V., van der Krogt, M., Koopman, H.F., Verdonschot, N., 2016. Sensitivity of subject-specific models to Hill muscle–tendon model parameters in simulations of gait. J. Biomech. 49, 1953–1960.

Carbone, V., Fluit, R., Pellikaan, P., van der Krogt, M., Janssen, D., Damsgaard, M., Vigneron, L., Feilkas, T., Koopman, H., Verdonschot, N., 2015. TLEM 2.0–A comprehensive musculoskeletal geometry dataset for subject-specific modeling of lower extremity. J. Biomech. 48, 734–741.

Cignoni, P., Callieri, M., Corsini, M., Dellepiane, M., Ganovelli, F., Ranzuglia, G., Year Meshlab: an open-source mesh processing tool. In Eurographics Italian Chapter Conference.

Consolaro, A., Ruperto, N., Bazso, A., Pistorio, A., Magni-Manzoni, S., Filocamo, G., Malattia, C., Viola, S., Martini, A., Ravelli, A., 2009. Development and validation of a composite disease activity score for juvenile idiopathic arthritis. Arthritis Care & Res. 61, 658–666.

Correa, T.A., Baker, R., Kerr Graham, H., Pandy, M.G., 2011. Accuracy of generic musculoskeletal models in predicting the functional roles of muscles in human gait. J. Biomech. 44, 2096–2105.

Correa, T.A., Pandy, M.G., 2011. A mass–length scaling law for modeling muscle strength in the lower limb. J. Biomech. 44, 2782–2789.

Damsgaard, M., Rasmussen, J., Christensen, S.T., Surma, E., de Zee, M., 2006. Analysis of musculoskeletal systems in the AnyBody Modeling System. Simul. Model. Pract. Theory 14, 1100–1111.

Davis, R., Ounpuu, S., Tyburski, D., Gage, J., 1991. A gait analysis data collection and reduction technique. Hum. Mov. Sci. 10, 575–587.

Delp, S.L., Anderson, F.C., Arnold, A.S., Loan, P., Habib, A., John, C.T., Guendelman, E., Thelen, D.G., 2007. OpenSim: open-source software to create and analyze dynamic simulations of movement. IEEE Trans. Biomed. Eng. 54, 1940–1950.

Delp, S.L., Loan, J.P., Hoy, M.G., Zajac, F.E., Topp, E.L., Rosen, J.M., 1990. An interactive graphics-based model of the lower extremity to study orthopaedic surgical procedures. IEEE Trans. Biomed. Eng. 37, 757–767.

Dumas, R., Aissaoui, R., Mitton, D., Skalli, W., de Guise, J.A., 2005. Personalized body segment parameters from biplanar low-dose radiography. IEEE Trans. Biomed. Eng. 52, 1756–1763.

Erdemir, A., Guess, T.M., Halloran, J.P., Modenese, L., Reinbolt, J.A., Thelen, D.G., Umberger, B.R., 2016. Commentary on the integration of model sharing and reproducibility analysis to scholarly publishing workflow in computational biomechanics. IEEE Trans. Biomed. Eng. 63, 2080–2085.

Fregly, B., Besier, T.F., Lloyd, D.G., Delp, S.L., Banks, S.A., Pandy, M.G., D'Lima, D.D., 2012. Grand challenge competition to predict in vivo knee loads. J. Orthop. Res. 30, 503–513.

Gerus, P., Sartori, M., Besier, T.F., Fregly, B.J., Delp, S.L., Banks, S.A., Pandy, M.G., D'Lima, D.D., Lloyd, D.G., 2013. Subject-specific knee joint geometry improves predictions of medial tibiofemoral contact forces. J. Biomech. 46, 2778–2786.

Hainisch, R., Gfoehler, M., Zubayer-Ul-Karim, M., Pandy, M.G., 2012. Method for determining musculotendon parameters in subject-specific musculoskeletal models of children developed from MRI data. Multibody Syst. Dynam. 28, 143–156.

Handsfield, G.G., Meyer, C.H., Hart, J., Abel, M., Blemker, S.S., 2014. Relationships of 35 lower limb muscles to height and body mass quantified using MRI. J. Biomech. 47, 631–638.

Hannah, I., Montefiori, E., Modenese, L., Prinold, J., Viceconti, M., Mazzà, C., 2017. Sensitivity of a juvenile subject-specific musculoskeletal model of the ankle joint to the variability of operator-dependent input. Proc. Inst. Mech. Eng. [H] 231, 415–422.

Herzog, W., 1992. Sensitivity of muscle force estimations to changes in muscle input parameters using nonlinear optimization approaches. J. Biomech. Eng. 114, 267–268.

Hicks, J., Uchida, T., Seth, A., Rajagopal, A., Delp, S.L., 2014. Is my model good enough? Best practices for verification and validation of musculoskeletal models and simulations of human movement. J. Biomech. Eng. 137.

Horn, B.K., 1987. Closed-form solution of absolute orientation using unit quaternions. JOSA A 4, 629–642.

Isman, R.E., Inman, V.T., 1968. Anthropometric studies of the human foot and ankle. Bullet. Prosthetics Res. 10 (11), 97–129.

Kainz, H., Modenese, L., Lloyd, D.G., Maine, S., Walsh, H.P.J., Carty, C.P., 2016. Joint kinematic calculation based on clinical direct kinematic versus inverse kinematic gait models. J. Biomech. 49, 1658–1669.

Kapandji, I.A., 1987. The physiology of the joints. Lower limb.

Kolk, S., Klawer, E.M.E., Schepers, J., Weerdesteyn, V., Visser, E.P., Verdonschot, N., 2015. Muscle activity during walking measured using 3D MRI segmentations and [18F]-fluorodeoxyglucose in combination with positron emission tomography. Med. Sci. Sports Exerc. 47, 1896–1905.

Kutzner, I., Heinlein, B., Graichen, F., Bender, A., Rohlmann, A., Halder, A., Beier, A., Bergmann, G., 2010. Loading of the knee joint during activities of daily living measured in vivo in five subjects. J. Biomech. 43, 2164–2173.

Lanni, S., Bovis, F., Ravelli, A., Viola, S., Magnaguagno, F., Pistorio, A., Michele Magnano, G., Martini, A., Malattia, C., 2016. Delineating the application of ultrasound in detecting synovial abnormalities of the subtalar joint in juvenile idiopathic arthritis. Arthrit. Care & Res. 68, 1346–1353.

Lieber, R.L., Friden, J., 2000. Functional and clinical significance of skeletal muscle architecture. Muscle & Nerve 23, 1647–1666.

Malattia, C., Consolaro, A., Pederzoli, S., Madeo, A., Pistorio, A., Mazzoni, M., Mattiuz, C., Magnano, G.M., Viola, S., Buoncompagni, A., Palmisani, E., Hasija, R., Ruperto, N., Ravelli, A., Martini, A., 2013. MRI versus conventional measures of disease activity and structural damage in evaluating treatment efficacy in juvenile idiopathic arthritis. Ann. Rheum. Dis. 72, 363–368.

Marra, M.A., Vanheule, V., Fluit, R., Koopman, B.H., Rasmussen, J., Verdonschot, N., 2015. A subject-specific musculoskeletal modeling framework to predict in vivo mechanics of total knee arthroplasty. J. Biomech. Eng. 137, 020904.

Modenese, L., Ceseracciu, E., Reggiani, M., Lloyd, D.G., 2016. Estimation of musculotendon parameters for scaled and subject specific musculoskeletal models using an optimization technique. J. Biomech. 49, 141–148.

Modenese, L., Phillips, A.T.M., Bull, A.M.J., 2011. An open source lower limb model: hip joint validation. J. Biomech. 44, 2185–2193.

Moller, T., Reif, E., 2007. Pocket Atlas of Cross-sectional Anatomy CT and MRI: Head, Neck, Spine, and Joints. Thieme.

Montefiori, E., Modenese, L., Viceconti, M., Mazzà, C., Year A subject-specific foot model for the estimation of subtalar joint kinematics. In: XXVI Congress of the International Society of Biomechanics, Brisbane.

Navacchia, A., Myers, C., Rullkoetter, P.J., Shelburne, K.B., 2015. Prediction of in vivo knee joint loads using a global probabilistic analysis. J. Biomech. Eng.

Parenti-Castelli, V., Sancisi, N., 2013. Synthesis of spatial mechanisms to model human joints, 21st Century Kinematics. Springer, 49–84.

Parr, W.C.H., Chatterjee, H.J., Soligo, C., 2012. Calculating the axes of rotation for the subtalar and talocrural joint using 3D bone reconstructions. J. Biomech. 45, 1103–1107.

Pataky, T.C., Robinson, M.A., Vanrenterghem, J., 2013. Vector field statistical analysis of kinematic and force trajectories. J. Biomech. 46, 2394–2401.

Prinold, J.I., Mazzà, C., Di Marco, R., Hannah, I., Malattia, C., Magni-Manzoni, S., Petrarca, M., Ronchetti, A., Tanturri de Horatio, L., van Dijkhuizen, E.H.P., Wesarg, S., Viceconti, M., 2016. A patient-specific foot model for the estimate of ankle joint forces in patients with juvenile idiopathic arthritis. Ann. Biomed. Eng. 44, 247–257.

Ravelli, A., Martini, A., 2007. Juvenile idiopathic arthritis. The Lancet 369, 767–778.

Roth, J., Ravagnani, V., Backhaus, M., Balint, P., Bruns, A., Bruyn, G.A., Collado, P., De la Cruz, L., Guillaume-Czitrom, S., Herlin, T., 2016. Preliminary definitions for the sonographic features of synovitis in children. Arthrit. Care Res.

Sancisi, N., Parenti-Castelli, V., 2011. A new kinematic model of the passive motion of the knee inclusive of the patella. J. Mech. Robot. 3, 041003.

Saraswat, P., Andersen, M.S., MacWilliams, B.A., 2010. A musculoskeletal foot model for clinical gait analysis. J. Biomech. 43, 1645–1652.

Scheys, L., Desloovere, K., Spaepen, A., Suetens, P., Jonkers, I., 2011. Calculating gait kinematics using MR-based kinematic models. Gait & Posture 33, 158–164.

Scheys, L., Loeckx, D., Spaepen, A., Suetens, P., Jonkers, I., 2009. Atlas-based non-rigid image registration to automatically define line-of-action muscle models: a validation study. J. Biomech. 42, 565–572.

Scheys, L., Spaepen, A., Suetens, P., Jonkers, I., 2008. Calculated moment-arm and muscle-tendon lengths during gait differ substantially using MR based versus rescaled generic lower-limb musculoskeletal models. Gait & Post 28, 640–648.

Scovil, C.Y., Ronsky, J.L., 2006. Sensitivity of a Hill-based muscle model to perturbations in model parameters. J. Biomech. 39, 2055–2063.

Siegler, S., Toy, J., Seale, D., Pedowitz, D., 2014. The Clinical Biomechanics Award 2013 – presented by the International Society of Biomechanics: new observations on the morphology of the talar dome and its relationship to ankle kinematics. Clin. Biomech. 29, 1–6.

Stebbins, J., Harrington, M., Thompson, N., Zavatsky, A., Theologis, T., 2006. Repeatability of a model for measuring multi-segment foot kinematics in children. Gait & Post. 23, 401–410.

Steele, K.M., DeMers, M.S., Schwartz, M.H., Delp, S.L., 2012a. Compressive tibiofemoral force during crouch gait. Gait & Post. 35, 556–560.

Steele, K.M., van der Krogt, M.M., Schwartz, M.H., Delp, S.L., 2012b. How much muscle strength is required to walk in a crouch gait? J. Biomech. 45, 2564–2569.

Steger, S., Kirschner, M., Wesarg, S., 2012. Articulated atlas for segmentation of the skeleton from head & neck CT datasets. In: 9th IEEE International Symposium on Biomedical Imaging (ISBI). Barcelona, Spain.

Taddei, F., Ansaloni, M., Testi, D., Viceconti, M., 2007. Virtual palpation of skeletal landmarks with multimodal display interfaces. Inform. Health Social Care 32, 191–198.

Taddei, F., Martelli, S., Valente, G., Leardini, A., Benedetti, M.G., Manfrini, M., Viceconti, M., 2012. Femoral loads during gait in a patient with massive skeletal reconstruction. Clin. Biomech. 27, 273–280.

Thelen, D.G., 2003. Adjustment of muscle mechanics model parameters to simulate dynamic contractions in older adults. J. Biomech. Eng. 125, 70–77.

Valente, G., 2013. Subject-specific musculoskeletal models of the lower limbs for the prediction of skeletal loads during motion. Università di Bologna.

Valente, G., Crimi, G., Vanella, N., Schileo, E., Taddei, F., 2017. nmsBuilder: freeware to create subject-specific musculoskeletal models for OpenSim. Comput. Methods Programs Biomed. 152, 85–92.

Valente, G., Pitto, L., Testi, D., Seth, A., Delp, S.L., Stagni, R., Viceconti, M., Taddei, F., 2014. Are subject-specific musculoskeletal models robust to the uncertainties in parameter identification? PLoS ONE 9, e112625.

van Sint Jan, S., 2007. Color atlas of skeletal landmark definitions: guidelines for reproducible manual and virtual palpations. Elsevier Health Sciences, ISBN 1455725196.

Weijs, W.A., Hillen, B., 1985. Cross-sectional areas and estimated intrinsic strength of the human jaw muscles. Acta Morphologica Neerlando-Scandinavica 23, 267–274.

White, D., Woodard, H., Hammond, S., 1987. Average soft-tissue and bone models for use in radiation dosimetry. Brit. J. Radiol. 60, 907–913.

Please cite this article in press as: Modenese, L., et al. Investigation of the dependence of joint contact forces on musculotendon parameters using a codified workflow for image-based modelling. J. Biomech. (2018), https://doi.org/10.1016/j.jbiomech.2018.03.039

Winby, C.R., Lloyd, D.G., Kirk, T.B., 2008. Evaluation of different analytical methods for subject-specific scaling of musculotendon parameters. J. Biomech. 41, 1682–1688.

Wu, G., Siegler, S., Allard, P., Kirtley, C., Leardini, A., Rosenbaum, D., Whittle, M., D'Lima, D.D., Cristofolini, L., Witte, H., Schmid, O., Stokes, I., 2002. ISB recommendation on definitions of joint coordinate system of various joints for the reporting of human joint motion - part I: ankle, hip, and spine. J. Biomech. 35, 543–548.

Yin, L., Chen, K., Guo, L., Cheng, L., Wang, F., Yang, L., 2015. Identifying the functional flexion-extension axis of the knee: an in-vivo kinematics study. PloS One 10, e0128877.

Zajac, F.E., 1989. Muscle and tendon: properties, models, scaling, and application to biomechanics and motor control. Crit. Rev. Biomed. Eng. 17, 359–411.

Zhang, J., Sorby, H., Clement, J., Thomas, C.D.L., Hunter, P., Nielsen, P., Lloyd, D., Taylor, M., Besier, T., 2014. The MAP Client: User-Friendly Musculoskeletal Modelling Workflows. Biomed. Simul. Springer, 182–192.

Please cite this article in press as: Modenese, L., et al. Investigation of the dependence of joint contact forces on musculotendon parameters using a codified workflow for image-based modelling. J. Biomech. (2018), https://doi.org/10.1016/j.jbiomech.2018.03.039